

Chapter 2

Forcings

Kyung-Ae Park, Kyung-Il Chang, Hanna Na and Uk-Jae Jung

Abstract The East Sea (Japan Sea) is strongly influenced by the Asian monsoon with prevalent northerly and southerly winds in winter and summer, respectively. It gains heat from April to August and loses heat in other seasons with annual net heat loss ranging from 25 to 108 W m⁻². Extremely strong winds of severe Siberian cold-air outbreaks typify the winter season from December to February, which occasionally results in cold bottom water formation. A spatially distinct pattern of wind stress curl during the outbreak periods appears south of Vladivostok and near East Korea Bay. The cold-air outbreaks result in significant surface heat losses through sensible and latent heat fluxes exceeding 500 W m⁻², which was estimated to be even larger, as high as 1000 W m⁻², during a deep convection period in winter. Wintertime surface heat loss is also an important factor in deep penetration of frontal subduction, resulting in the formation of East Sea Intermediate Water found south of the subpolar front. Net heat loss at the sea surface in the East Sea is compensated by its warm inflow-outflow system. Inflow of the Tsushima Warm Current through the Korea Strait (2.6 Sv), which is balanced with outflows through the Tsugaru Strait and the Soya Strait, exhibits large

K.-A. Park (✉)

Department of Earth Science Education, Seoul National University, Seoul 151-748,
Republic of Korea

e-mail: kapark@snu.ac.kr

K.-A. Park · K.-I. Chang

Research Institute of Oceanography, Seoul National University, Seoul 151-742,
Republic of Korea

K.-I. Chang · U.-J. Jung

School of Earth and Environmental Sciences, Seoul National University, Seoul 151-742,
Republic of Korea

e-mail: ujjung@curl.snu.ac.kr

H. Na

Faculty of Science, Hokkaido University, Sapporo, Hokkaido 060-0810, Japan

e-mail: hna@mail.sci.hokudai.ac.jp

volume transports in summer to autumn and small in winter to spring with a range of about 1 Sv ($1 \text{ Sv} = 10^6 \text{ m}^3 \text{ s}^{-1}$). While the mean transport is larger in the Tsugaru Strait compared to that in the Soya Strait, the seasonal variability is larger in the Soya Strait.

Keywords Sea surface wind • Surface heat flux • Volume transport • Tsushima Warm Current • Korea Strait • Tsugaru Strait • Soya Strait • East Sea (Japan Sea)

2.1 Introduction

The East Sea has many characteristics similar to those of the global ocean and may be considered its miniature. There are remarkable atmospheric and oceanic forcings such as wind forcing, surface heat flux at the air-sea interface, and boundary flux through straits, which have strongly affected the basin-wide surface-to-deep-water circulations, formation and distribution of water masses, and many other properties of the East Sea. It is almost impossible to discuss substantial changes in water masses, currents, and circulations without a priori knowledge of the spatial and temporal variability of the fundamental forcing fields over the East Sea. Thus, in the following sections, we have attempted to review the previous literature and recent results on wind forcing (Sect. 2.2), surface heat flux (Sect. 2.3), and boundary flux (Sect. 2.4). Section 2.5 is a summary, and a discussion of remaining issues.

2.2 Surface Wind

2.2.1 Accuracy of Satellite Scatterometer Wind Vectors

Satellite scatterometers have measured near-surface wind velocity vectors under all weather conditions with accuracy of less than 2 m s^{-1} in speed and 20° in direction and spatial resolution of 25 km (Jet Propulsion Laboratory 1998). Scatterometers such as NASA Scatterometer (NSCAT) of the ADvanced Earth Observing Satellite (ADEOS), SeaWinds of the Quick Scatterometer (QuikSCAT), and the Advanced Scatterometer (ASCAT) of Europe's Meteorological Operational Satellite Program—A have been successfully operated with relatively high spatial and temporal coverage since September 1996.

Over the decade prior to the launch of satellite scatterometers in the 1990s, wind fields for the period 1978–1997 produced by Na et al. (1997), called ‘Na wind’ hereafter, was the most renowned in the scientific community and extensively utilized for diverse studies in the seas adjacent to Korea (e.g. Kim and Yoon 1996). Unlike automatic weather station (AWS) measurements, it is not based on direct measurements of wind vectors but on those indirectly calculated from the distribution of atmospheric pressure on daily weather maps using the Cardone model (Cardone 1969). The Na wind field has both similarity and dissimilarity to the scatterometer wind field. Comparing the two, the spatial structures are mostly

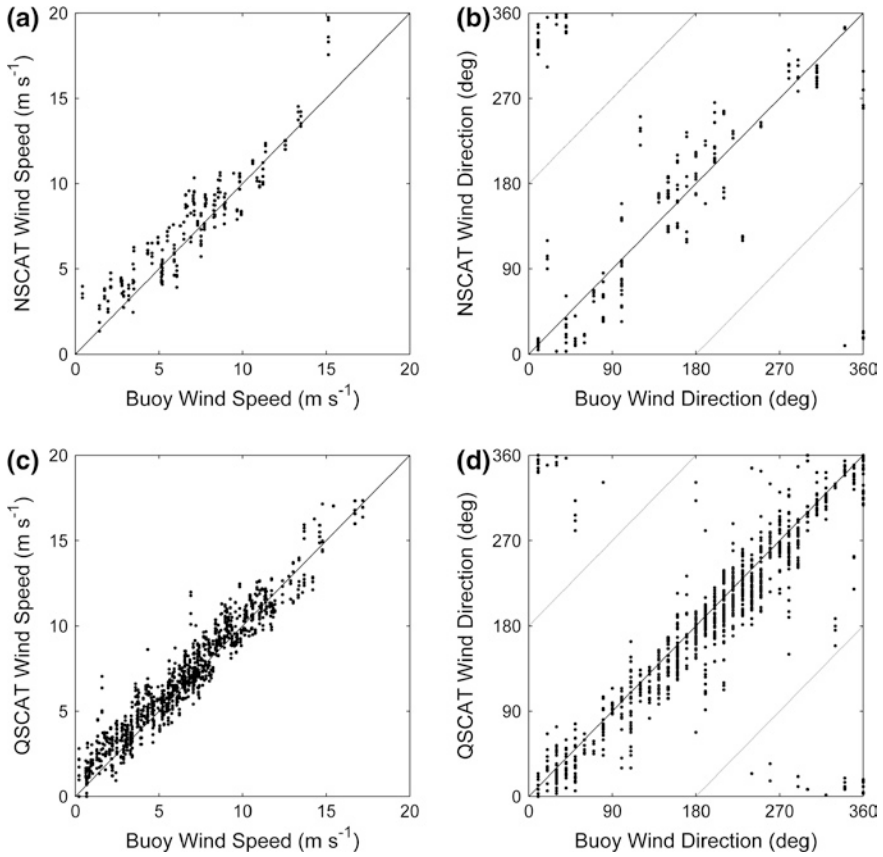


Fig. 2.1 Comparison of satellite-derived winds with winds from three Japan Meteorological Agency (JMA) buoys in the seas adjacent to Korea: **a** NSCAT wind speed, **b** NSCAT wind direction, **c** QuikSCAT wind speed, and **d** QuikSCAT wind direction (from Kim et al. 2005)

coherent on large basin-wide scales, but significant differences and energy loss are detected in the Na wind at spatial scales less than 100 km (Park et al. 2003).

Comparison of satellite scatterometer-derived wind speeds from NSCAT and QuikSCAT/SeaWinds with buoy-measured wind speeds reveals relatively small root-mean-squared (rms) errors with a range of 0.9–1.3 m s^{-1} in the East Sea; this meets the scatterometer mission error limit requirement of 2 m s^{-1} as shown in Fig. 2.1 (Ebuchi 1997; Lee 1998; Park et al. 2003; Kim et al. 2005). However, scatterometer wind directions show large rms errors of 15°–40° due to ambiguity problems, random and systematic errors, and the uncertainty of geophysical model functions (Freilich 1997; Park et al. 2003). Regional biases of wind vectors in the East Sea are large at low wind speeds in particular; these biases depend on wind speed and atmospheric stability in the marine-atmospheric boundary layer (MABL) (Park and Cornillon 2002; Chelton et al. 2004; Park et al. 2006a). In addition, scatterometers have saturation problems at high wind speeds causing an underestimation of wind speeds when compared with buoy measurements of

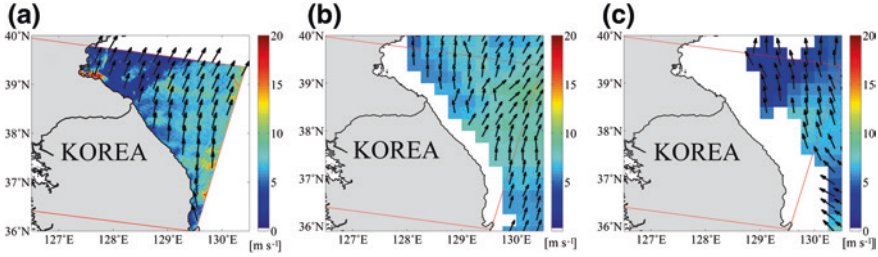


Fig. 2.2 Distribution of wind speed (color scale in m s^{-1}) and direction (arrow) off the east coast of Korea from **a** ALOS PALSAR, **b** QuikSCAT, and **c** ASCAT, on the same date (11 August 2007), where the red box indicates the boundary of ALOS PALSAR observations (redrawn from Kim et al. 2012)

winds (Liu and Xie 2006). Since the oceanic near-surface wind field also plays an important role in the estimation of latent heat flux and sensible heat flux, it should be continuously produced with high quality to reduce uncertainty in the estimation of net heat flux in the East Sea.

Since a satellite scatterometer observes winds at relatively low resolution of about 25 km, scatterometer data are not readily applicable in coastal areas. By contrast, Synthetic Aperture Radar (SAR) can provide a high-resolution wind field even within 25 km from the coast (Fig. 2.2). In the East Sea, some studies have been performed to validate the SAR-observed winds by comparison with winds from moored buoys, AWS near the coast, and numerical models (Isoguchi and Kawamura 2007). Overall, the rms errors of wind speeds from C-band and L-band SARs meet the error limit of 2 m s^{-1} in the East Sea (Kim and Moon 2002; Kim et al. 2010, 2012; Kim and Park 2011). The high-resolution coastal winds of the East Sea are anticipated to promote deep understanding of physical and biological processes at the coastal areas.

2.2.2 Spatial and Temporal Variability of Near-Surface Winds

Figure 2.3 shows the distribution of monthly-mean wind vectors calculated using QuikSCAT data from 2000 through 2008. The scatterometer wind fields reveal detailed spatial structures with large spectral energy even at high wavenumbers (Lee 1998; Park et al. 2003). The monthly-mean speeds range from 3 to 12 m s^{-1} over the basin. Overall, the speeds are larger during the wintertime, with values greater than 8 m s^{-1} beginning in November and reaching a peak in January ($>10 \text{ m s}^{-1}$), particularly south of Vladivostok and along the Primorye coast. Northwestern cold-air outbreaks through Vladivostok in winter cause the formation of cold bottom water in the East Sea and drive a cyclonic circulation in the Japan Basin (e.g. Kawamura and Wu 1998; Chen et al. 2001; Chu et al. 2001; Kim et al. 2002; Dorman et al. 2004). Strong winds also appear over East Korea Bay

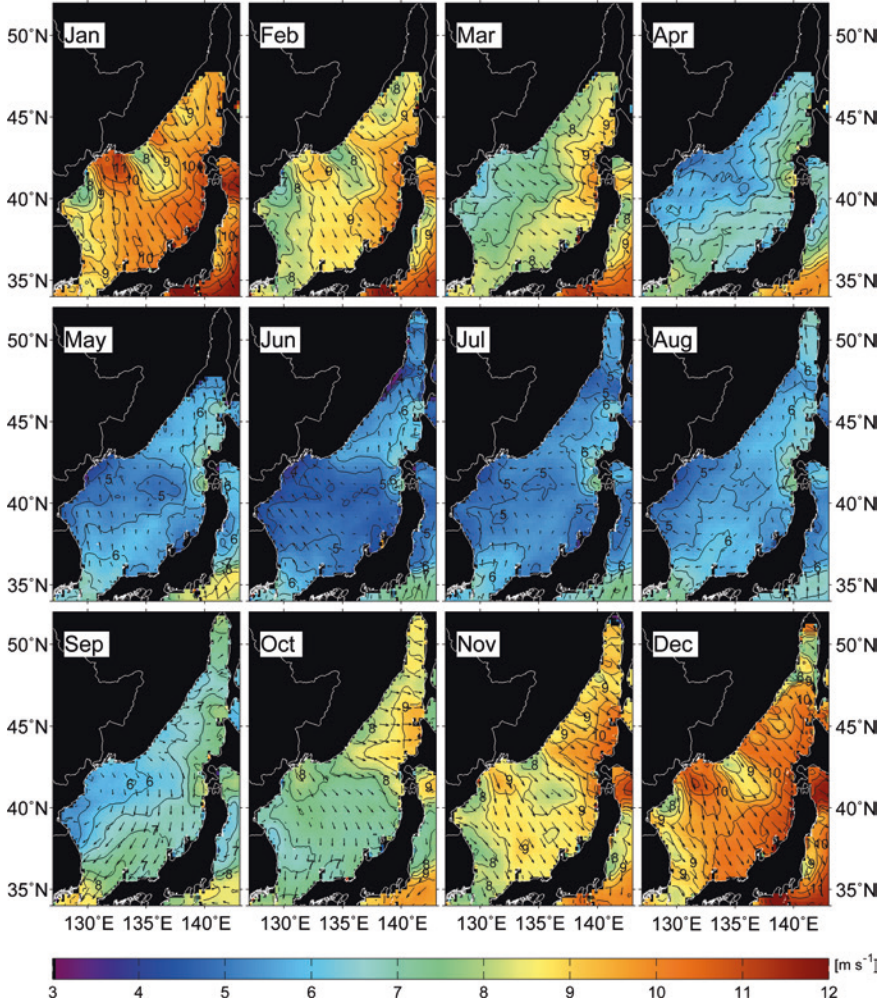


Fig. 2.3 Spatial distribution of monthly-mean wind vectors from 9 years of QuikSCAT data for the period from 2000 to 2008 over the East Sea

(see Fig. 1.1) (Park et al. 2003; Nam et al. 2005). Southerly winds begin to blow in April, with lowest speeds of less than 5 m s^{-1} in June, and last into August (Fig. 2.3) when the wind direction changes from southerly to northerly. Northerly winds continue through fall and winter until March of the next year.

Northerly winds passing through the orographic gap near Vladivostok begin in October, become stronger at $\sim 10 \text{ m s}^{-1}$ in December, achieve greatest strength of about 12 m s^{-1} as cold-air outbreaks in January, and last, at $\sim 8 \text{ m s}^{-1}$, until February (Fig. 2.3). During such cold outbreaks, the 0°C surface air isotherm extends well southward of 40°N , the surface heat losses in the center of the East

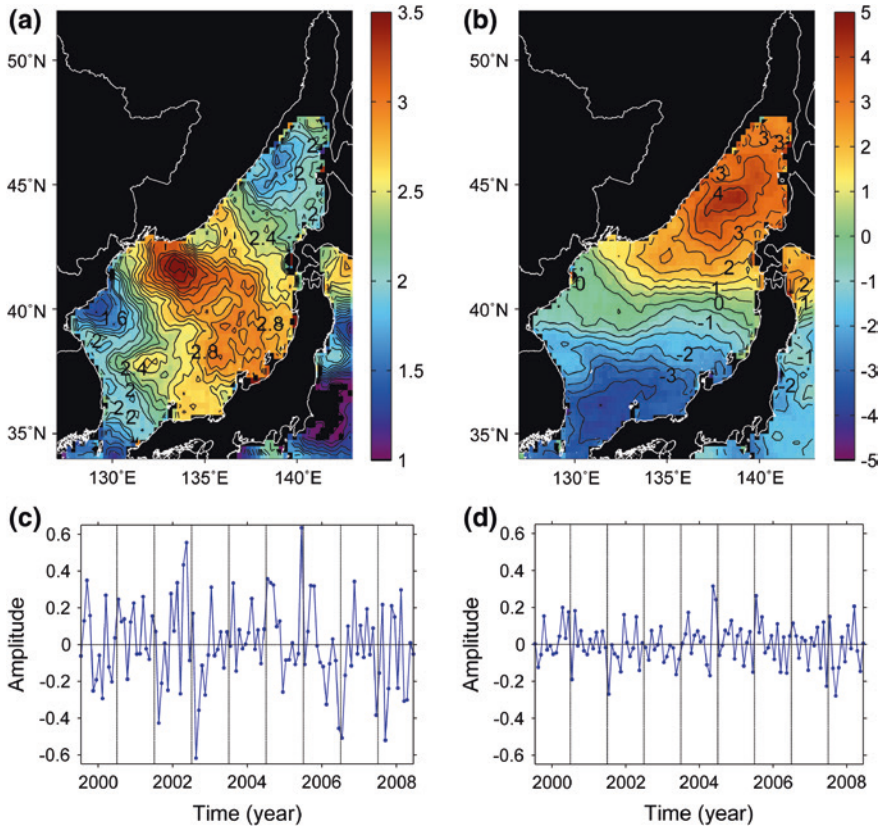


Fig. 2.4 **a** First and **b** second EOF modes of monthly-mean QuikSCAT wind speeds over the East Sea from 2000 to 2008, and **c–d** their time-varying amplitudes

Sea can exceed 600 W m^{-2} , and cloud streets with individual roll clouds cover most of the East Sea, extending from the Russian coast to Honshu (Dorman et al. 2004). The average number of strong cold-air outbreaks per winter (November–March) season is about 13, occupying 39 % of the winter period and contributing 43 % of the net heat loss from the East Sea (Dorman et al. 2004). More details about the surface buoyancy flux are in Sect. 2.3.

Figure 2.4a shows the first EOF mode of 9-year QuikSCAT wind speed anomalies over the East Sea from 2000 through 2008, accounting for 44.3 % of the total variance. Overall, it represents the strong winds from the continental side to the offshore region during cold-air outbreaks in winter. The winds are spatially shielded by mountainous land masses between Vladivostok and the north-eastern part off the Primorye coast, producing low speeds in that region (Park et al. 2003). The time-varying amplitudes usually reach a peak in January each year (Fig. 2.4c). Large values over the southeastern region near the Japanese coast are related to relatively high wind speeds due to strengthening of unstable

condition within the MABL (Park and Cornillon 2002; Chelton et al. 2004; Park et al. 2006a; Shimada and Kawamura 2006). The second EOF mode (Fig. 2.4b), explaining 10.1 % of the QuikSCAT wind variance, is dominant in the region between the Russian coast and Hokkaido from 40°N to 48°N in winter. The impact of such wind forcing on oceanic circulation has not been studied vigorously and should be studied in the future.

2.2.3 Wind Stress and Its Curl

Nam et al. (2005) analyzed near-shore and off-shore wind stress and showed typical amplitudes of wind stress off the east coast of Korea in the seasonal (>90 days), intra-seasonal (20–90 days), and synoptic (2–20 days) bands are 0.20, 0.03, and 0.04–0.18 N m^{-2} , respectively. The synoptic-band wind stress shows seasonal modulation by becoming stronger in winter (0.5–0.6 N m^{-2}) than in summer. The wind stress curl causes a pair of positive and negative values on the left and right sides of the downwind air flow, owing to the intensification of winds through the orographic gap near Vladivostok (Kawamura and Wu 1998; Park et al. 2003; Dorman et al. 2004; Nam et al. 2005; Shimada and Kawamura 2006). Another paired structure of positive/negative curl is found off Wonsan over East Korea Bay, for which the mechanism is similar to that south of Vladivostok, being driven by winds through an orographic gap between mountains (Park et al. 2003; Nam et al. 2005). Wind stress curl fields result also from accelerations and decelerations of wind as it blows over subpolar fronts in the central part of the East Sea (Shimada and Kawamura 2006).

The positive wind stress curl of the dipole structure occupying most of the East Sea in winter generates a large basin-wide cyclonic circulation (Yoon et al. 2005). The cyclonic wind stress curl in East Korea Bay may play an important role in the separation of the East Korea Warm Current (EKWC) (Kim and Yoon 1996; Yoon et al. 2005). Trusenkov et al. (2009) indicated that wind stress curl can be an additional factor forcing the Tsushima Warm Current (TWC) to branch off at the Korea Strait into the EKWC and the Offshore Branch. Sensitivity of the circulation to the different wind forcings has proved to be significant, which means the wind forcing, along with surface buoyancy forcing, is substantial in determining the different patterns and magnitudes of the basin-wide circulation (Hogan and Hulbert 2000).

2.3 Surface Heat Flux

2.3.1 Comparison of Heat Flux Estimates

Heat flux estimates in the East Sea are available from several studies (Table 2.1). The surface heat fluxes are usually computed by means of bulk formulas using atmospheric and marine surface data at the air-sea interface. The net heat flux Q_{net}

Table 2.1 Comparisons of summertime (Sum.; June–August), wintertime (Win.; December–February), and annual mean (Ann.) latent, sensible, and net heat fluxes (W m^{-2}) in the East Sea

Sources	Periods	Q_e			Q_h			Q_{net}		
		Sum.	Win.	Ann.	Sum.	Win.	Ann.	Sum.	Win.	Ann.
Kato and Asai (1983)	78–79	–29	–169	–102	5	–132	–47			–35
Kondo et al. (1994)	65–90	–26	–124	–78	5	–88	–31			–25
Park et al. (1995)	61–90	–17	–161	–90	2	–97	–32			–51
Hirose et al. (1996)	60–90	–35	–143	–93	1	–108	–40	113.3	–251	–53
Ahn et al. (1997)	80–94			–141			–41			–90
Na et al. (1999)	78–95	–42 ^a	–172 ^a	–114 ^a	–4 ^a	–144 ^a	–60 ^a	92 ^a	–332 ^a	–108 ^a
Hong et al. (2005)	88–00	–48	–144	–108	0.5	–79	–32			–70
Dorman et al. (2004, 2005)	Summer	–27/–28/5	–160/–69		4/–3/7	–142/–41		137/–138	–295/–77	
	5/19/99–6/02/00									
	6/24/99–7/18/99									
	7/19/99–8/11/99									
	Winter									
	1/17/00–2/04/00									
	3/02/00–3/16/00									
OAFlux	89–09	–28.6	–163.1	–97.7	2.2	–116.9	–43.9	130.7	–276	–59
ECMWF	91–01	–28.4	–145.2	–95.1	0	–106.3	–52.8	154.4	–263.7	–47.6

Flux estimates from the OAFlux products and ECMWF model results are also shown

^aValues estimated from figures, by eye

is the sum of four components, $Q_{\text{net}} = Q_s + Q_b + Q_h + Q_e$, where Q_s is the net shortwave radiation flux, Q_b the net long wave radiation flux, Q_h the sensible heat flux, and Q_e the latent heat flux. Different parameterizations were used for each of these components. As a sign convention, positive (negative) heat flux components denote oceanic heat gain (loss).

Heat flux estimates in gridded boxes with 0.2° – 2° resolutions based on different bulk formulas and long-term averaged input variables show considerable differences (Table 2.1, Fig. 2.5). We have also compared those previous estimates with long-term mean heat fluxes from 1991 to 2001 produced by the European Centre for Medium-range Weather Forecast (ECMWF) model (Dorman et al. 2005), and from 1989 to 2009 obtained from the Objectively Analyzed air-sea Fluxes (OAFlux) project at the Woods Hole Oceanographic Institution (Yu and Weller 2007). The annual climatological Q_{net} , winter Q_h , and winter Q_e from those estimates all show negative values, indicating oceanic heat loss, with amplitudes ranging 25–108, 79–144, and 124–172 W m^{-2} , respectively. The long-term mean Q_{net} values from the ECMWF model, OAFlux products, Park et al. (1995), and Hirose et al. (1996) (HKY96 hereafter) all show similar values of about -50 W m^{-2} (corresponding to about 0.05 PW over the entire East Sea), which is about the same as the surface heat loss over the East China Sea (0.04 PW; Liu et al. 2010). Net heat losses in Kato and Asai (1983) and Kondo et al. (1994), however, are smaller ranging from -35 to -25 W m^{-2} . The other studies reported larger-magnitude estimates between -108 and -70 W m^{-2} , mainly due to their larger winter Q_h or Q_e (Ahn et al. 1997; Na et al. 1999 (NSL99 hereafter); Hong et al. 2005). The relatively wide range of the long-term estimates may arise from differences of datasets used in the calculations, parameterizations used in the bulk formulas, temporal resolutions of input data (NSL99), and different time periods reflecting interannual variation of the fluxes. The range of interannual variation is from about -35 to -22 W m^{-2} with a peak-to-peak difference of -13 W m^{-2} , according to a time series of annual mean Q_{net} from the OAFlux product (not shown); this implies that the flux discrepancies in Table 2.1 are not due to interannual variation of the heat fluxes. Summer Q_h and Q_e magnitudes are only about 1–6 and 11–33 % of their respective winter values, and the large heat loss in winter is caused by the dry and cold Siberian cold air mass sweeping over the warm sea surface.

2.3.2 Temporal Variations

The climatological annual cycles of heat fluxes obtained from the ECMWF model between 1991 and 2001 (Dorman et al. 2005) are shown in Fig. 2.5 together with those from the OAFlux products, HKY96, and NSL99. Also included are estimates from Dorman et al. (2004, 2005) based on highly accurate atmospheric datasets collected during surveys over the East Sea from research vessels. Mean Q_{net} values are positive from April to August with annual maximum heat gain between May and July, and negative from September to March with maximum heat loss

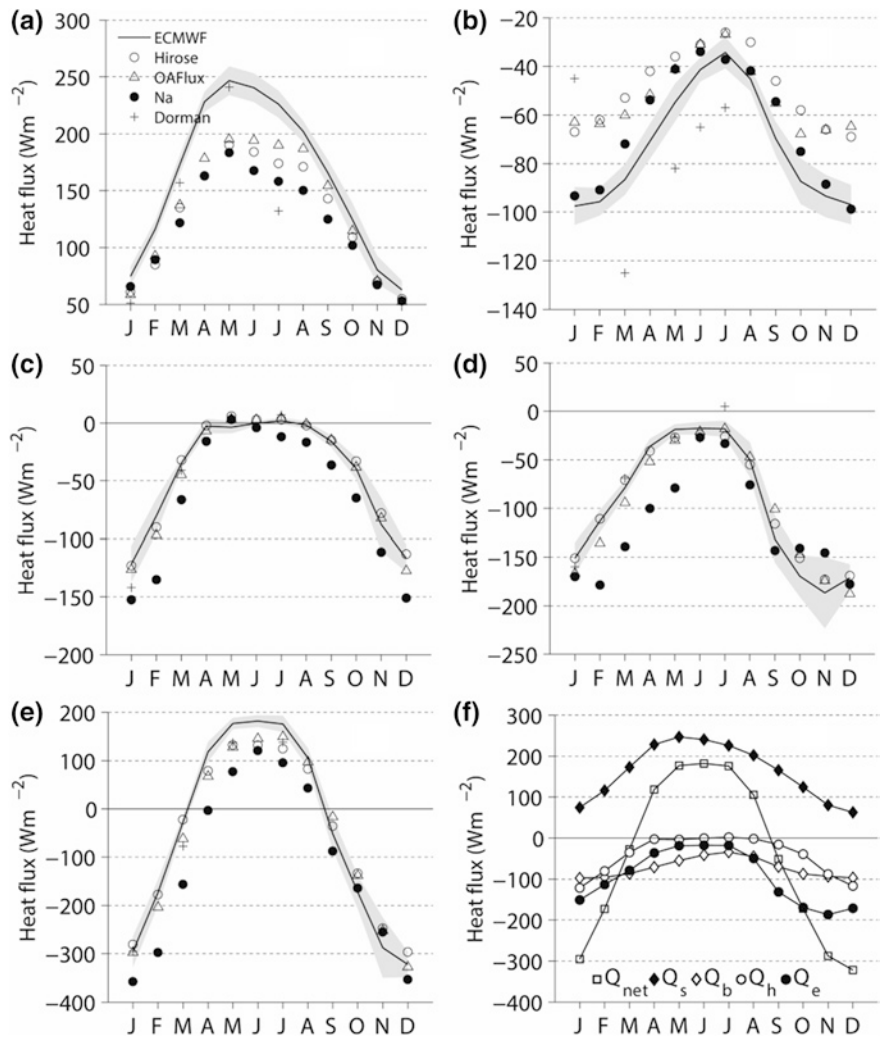


Fig. 2.5 Monthly-averaged heat flux components: **a** net shortwave flux (Q_s), **b** net longwave flux (Q_b), **c** sensible heat flux (Q_h), **d** latent heat flux (Q_e), **e** net heat flux (Q_{net}). Heat flux components based on ECMWF model results between 1991 and 2001 are shown as *solid lines*, with *shading* to indicate standard deviations. Both the monthly mean values and standard deviations for ECMWF model results are taken from Dorman et al. (2005). Heat flux components estimated by Hirose et al. (1996), Na et al. (1999), Dorman et al. (2004, 2005), and from OAFlux products are indicated by *open circles*, *closed circles*, *crosses*, and *triangles*, respectively. **f** Monthly-averaged heat flux components from ECMWF models results

in December and January (Fig. 2.5). In summer, surface heat flux is dominated by shortwave (Q_s) and longwave (Q_b) radiations, while the heat loss components (Q_b , Q_h , Q_e) show their annual minima due to reduced air-sea temperature differences and weak winds (Dorman et al. 2005). Major heat loss occurs in winter, especially through the latent (Q_e) and sensible (Q_h) heat fluxes. Heat losses due to sensible and latent fluxes between January and May estimated by NSL99 are larger than those from other estimates, yielding their larger net negative heat fluxes in those periods (see also Table 2.1).

The radiation components from the ECMWF model show large discrepancies compared with those components from other estimates. The ECMWF model results are characterized by large Q_s in summer and large heat loss through Q_b in winter. The Q_s in May 1999 (May 19–June 2) from Dorman et al. (2005) well matches the climatological Q_s from the ECMWF model. On the other hand, the Q_s value in July 1999 (July 19–August 11) shows a big discrepancy compared to the other climatological Q_s . The largest monthly Q_s values commonly occur in May due to the low cloud cover (HKY96). Compared to other estimates, the climatological monthly Q_b values from the ECMWF model and NSL99 have large-amplitude annual cycles due to large heat losses in winter.

Statistically significant negative Q_{net} trends occurred for 1984–2004 over the regions around the Kuroshio and the Kuroshio Extension, including the East Sea (Li et al. 2011). The negative trend over the East Sea was about $-10 \text{ W m}^{-2}/\text{decade}$ based on the OAFflux (Yu and Weller 2007). The negative Q_{net} trend was ascribed to the negative trend of Q_e due to an increase in the saturated specific humidity at the increasing sea surface temperature (Li et al. 2011). It should be noted that the trends based on a different dataset (National Oceanography Centre Southampton Flux Dataset v2.0, Berry and Kent 2009) show a negative trend in the southeastern East Sea, similar to the results from the OAFflux estimates, while a positive trend occurs in the northwestern East Sea.

The annual climatological Q_{net} over the East Sea is negative, the same as in western boundary current regions including the Kuroshio and the Kuroshio Extension (Han and Kang 2003; Li et al. 2011), meaning that, on average, the East Sea loses heat to the atmosphere. Further it implies that, under steady-state conditions, the East Sea receives heat from the surrounding seas by means of heat transported by the TWC through the Korea Strait (Isoda 1999; Han and Kang 2003). The estimated mean volume transport through the Korea Strait based on the surface heat flux is 2.20 Sv (HKY96), which is consistent with other independent estimates mentioned in Sect. 2.4.

2.3.3 Spatial Distribution

The spatial distribution of heat flux components shows significant spatial inhomogeneity especially in winter (HKY96). The long-term mean Q_{net} is negative over the East Sea except for a small region near the Russian coast, and its

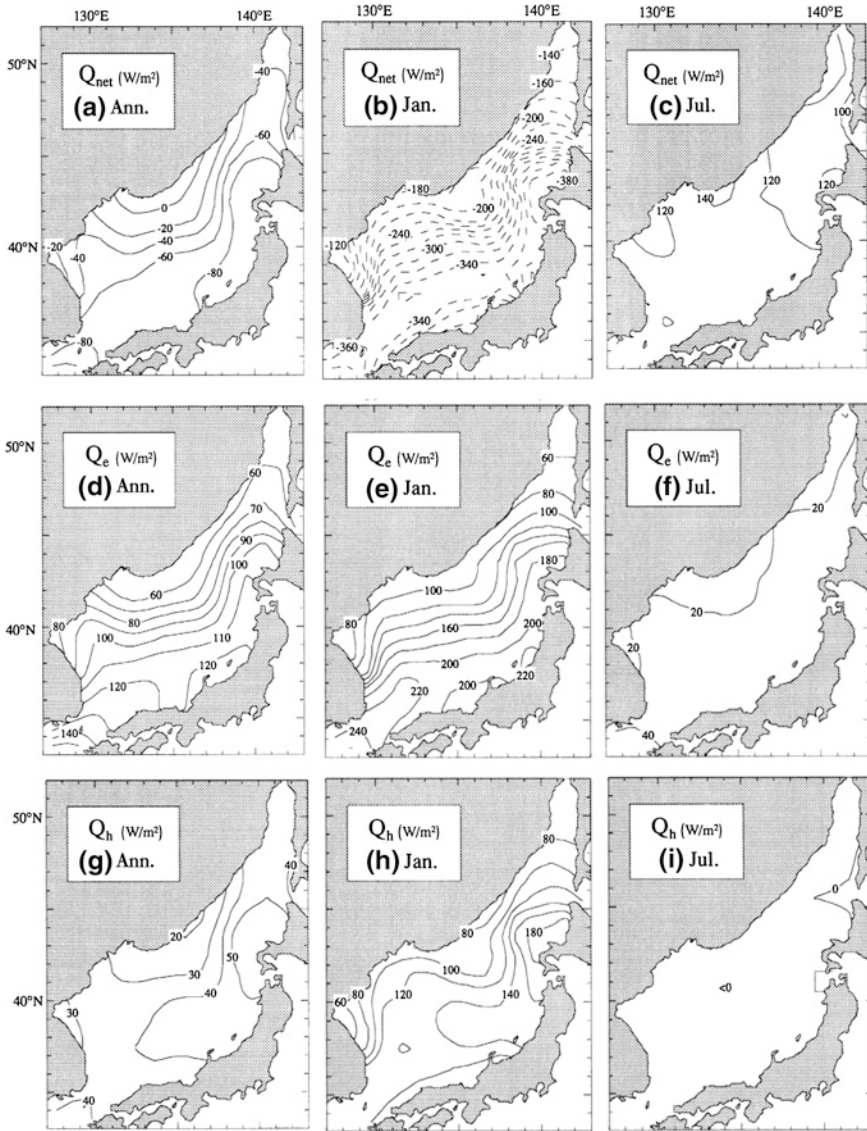


Fig. 2.6 Long-term annual mean heat flux components (*left panel*), and monthly mean heat flux components for January (*middle panel*) and for July (*right panel*). Q_{net} , Q_e , Q_h denote the sensible, latent, and net heat fluxes, respectively (Redrawn from Hirose et al. 1996)

spatial pattern is characterized by an increase in the heat loss toward the southeast (Fig. 2.6a). The large meridional difference in the Q_{net} field in winter (Fig. 2.6b) mainly determines the spatial pattern of the annual mean Q_{net} . And the winter-time heat losses due to the Q_e and Q_h (Fig. 2.6e, h) mainly account for the spatial

variation of the Q_{net} field. The spatial distribution of long-term mean Q_b (not shown) is relatively homogeneous. The spatial variation of Q_s is mainly determined by latitude and cloudiness, and the long-term mean Q_s value is large (small) in the southwestern (northeastern) part of the East Sea (not shown).

2.4 Boundary Flux

2.4.1 Korea Strait

The Korea Strait is about 180 km wide and 330 km long with a sill depth of 140 m. It is divided by Tsushima Island into a narrower (about 40 km) but deeper (about 220 m maximum) western channel and a wider (about 140 km) but shallower (about 110 m maximum) eastern channel (Fig. 2.7). A number of continuous observations since the late 1990s (Table 2.2) have revealed mean and temporal variations of the currents and transports in the Korea Strait (Chang et al. 2004 and references therein).

The TWC flows northeastward through the Korea Strait with a maximum speed near the center of the strait in its upstream region (to the south of Tsushima Island), while it splits into two branches in the downstream region (to the north of Tsushima Island, Fig. 2.8; see also Sect. 4.2). The core in the western channel is generally stronger than that in the eastern channel. A southwestward countercurrent is observed in the lee of Tsushima Island and is explained as part of a current-induced island wake (Takikawa et al. 2005; Teague et al. 2005;

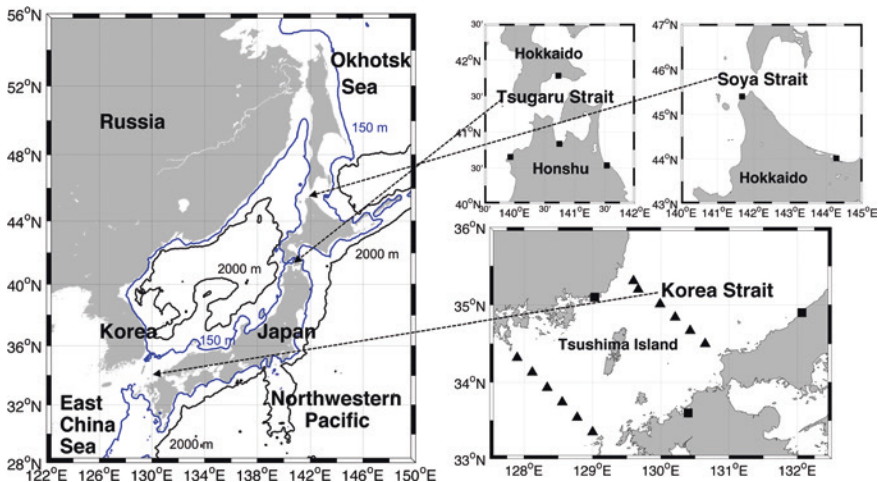


Fig. 2.7 Bottom topography (2000 and 150 m contours) and straits in the East Sea. *Squares* and *triangles* denote major tide gauge stations and bottom-mounted ADCP sites, respectively (from Teague et al. 2006 and references therein)

Table 2.2 Continuous observations in the straits

Straits	Periods	Methods	References
Korea	March 1998–present	Cable voltage measurement across the Strait	Kim et al. (2004)
	February 1997–present	Vessel-mounted ADCP across the Strait (Camellia)	Takikawa et al. (2005)
	May 1999–March 2000	Bottom-mounted ADCP across the Strait (LINKS program)	Teague et al. (2006) and references therein
	February 2002–present	High frequency radar around Tsushima Island	Yoshikawa et al. (2006)
Tsugaru	November 1999–March 2000	Vessel-mounted ADCP across the Strait	Ito et al. (2003)
	April 2000–December 2007	Vessel-mounted ADCP across the Strait	Kuroda et al. (2004)
Soya	August 2003–present	High frequency radar along the coast of Hokkaido	Ebuchi et al. (2006)

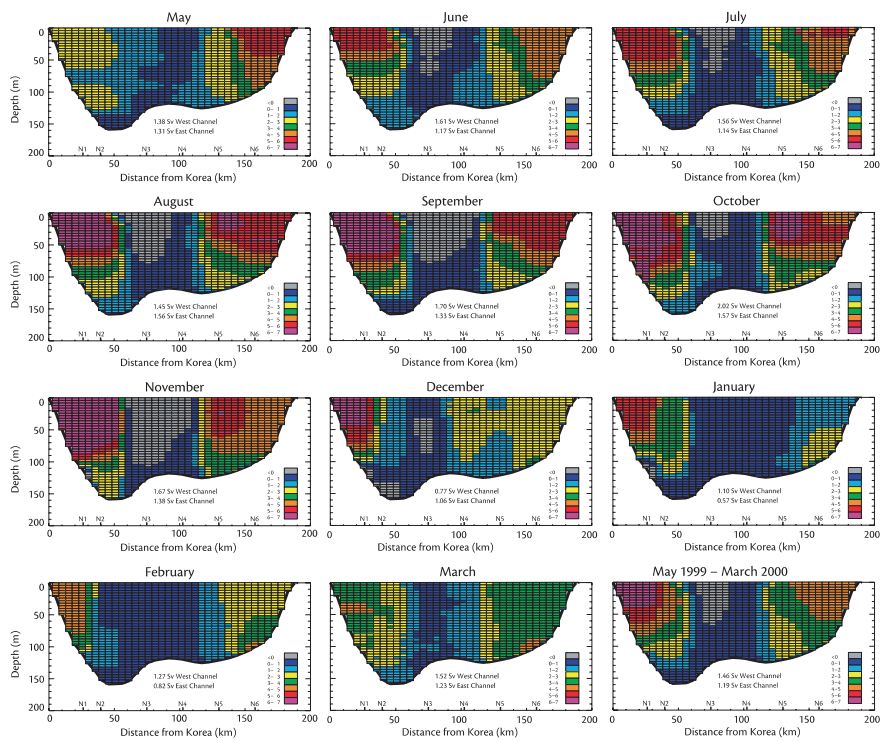


Fig. 2.8 Monthly averaged transports from May 1999 to March 2000, and averaged transport for the same period in the downstream region of the Korea Strait (to the north of Tsushima Island, Fig. 2.7) (from Teague et al. 2006). Units are $1 \text{ Sv} = 10^6 \text{ m}^3 \text{ s}^{-1}$. Each grid square is approximately 5-km across strait by 4 m in depth, except near the bottom where the depth dimension may be less

Yoshikawa et al. 2010). Tidal currents in the Korea Strait, which are stronger than those inside the East Sea, have maximum speed about $50\text{--}70\text{ cm s}^{-1}$ (Isobe et al. 1994; Teague et al. 2002; Takikawa et al. 2003). The maximum subtidal current is about 100 cm s^{-1} (Teague et al. 2002; Takikawa et al. 2005).

Mean volume transport through the Korea Strait is estimated to be about 2.6 Sv from various observational data (Isobe 2008 and references therein); this is roughly one-tenth of the mean positive (northeastward) transport of the Kuroshio in the East China Sea ($24.0 \pm 0.9\text{ Sv}$; Andres et al. 2008). Subinertial (2–10 days) variability is in the range of 2–3 Sv and shows amplification at the period of Helmholtz resonance (3–5 days) between the East Sea and the Pacific Ocean (Lyu et al. 2002). It is forced by atmospheric pressure disturbances because this subinertial period is too short for sea level inside the East Sea to respond isostatically, due to flow restrictions at the narrow and shallow straits (Nam et al. 2004; Lyu and Kim 2005; Park and Watts 2005; Kim and Fukumori 2008; see also Sect. 5.2). Seasonally, the volume transport is maximum from summer to autumn and minimum from winter to spring, with monthly standard deviation of about 1 Sv (Fig. 2.8; Teague et al. 2002; Lyu and Kim 2003; Takikawa et al. 2005). Interannual variability was reported to be as strong as seasonal variability (Kim et al. 2004).

Large-scale wind forcing over the North Pacific is known to be mainly responsible for the mean (Tsujino et al. 2008) and seasonal to interannual variability (Lyu and Kim 2005; Tsujino et al. 2008; Ma et al. 2012; see also Sect. 4.5). Local monsoonal wind forcing plays an additional role to modify the seasonal cycle of the TWC transport (Moon et al. 2009; Ma et al. 2012; Cho et al. 2013). It is notable that wind stress to the east of Soya Strait (over the Okhotsk Sea) was shown to be also important from the numerical modeling studies (Kim and Fukumori 2008; Tsujino et al. 2008).

The origin of the TWC is known to be the Kuroshio in the East China Sea (Nitani 1972; Lie et al. 1998) or the Taiwan Warm Current from the Taiwan Strait (Beardsley et al. 1985; Fang et al. 1991). Recent studies appear to agree that the contribution of the Kuroshio is larger in winter and that of the Taiwan Warm Current is larger in summer (Isobe 2008 and references therein). Cho et al. (2009) quantitatively showed that about 83 % of the volume transport through the Korea Strait is from the Kuroshio in winter and about 66 % comes from the Taiwan Warm Current in summer. Park et al. (2013) argued, however, that the branch current west of Kyushu could be overestimated in numerical modeling studies due to complex flow patterns, and consequently the Taiwan Warm Current is responsible for more than half of the TWC transport throughout the year.

In delivering warm water from the south, the TWC transports heat through the Korea Strait into the East Sea. Isobe et al. (2002), using observational data, calculated annual mean heat transport through the Korea Strait to be 0.17 PW ($1\text{PW} = 10^{15}\text{ W}$). A recent numerical modeling study showed that about 0.21 PW of heat should be transported through the Korea Strait, based on calculation of the oceanic heat budget over the East China Sea (Liu et al. 2010). These estimates are about one-tenth of the heat transport by the Kuroshio in the East China Sea (1.69 PW; Zhang et al. 2012).

Fresh water from the East China Sea is also delivered by the TWC to the East Sea through the Korea Strait. Isobe et al. (2002) estimated the freshwater transport as to be $3.3 \times 10^4 \text{ m}^3 \text{ s}^{-1}$ and suggested that at least 70 % of total river discharge around the Yellow and East China Seas flows into the East Sea. The Changjiang discharge accounts for about 90 % of this total river discharge and exhibits large seasonal variations with maximum in July and minimum in January (Chen et al. 1994). Salinity in the Korea Strait (both western and eastern channels) is correlated with the Changjiang discharge at interannual time scales (Senjyu et al. 2006). Wind stress over the East China Sea also affects salinity variation in the Korea Strait, particularly in the western channel, by modifying currents in the Cheju Strait (Senjyu et al. 2009).

The TWC also transports nutrients and other materials that greatly affect biological productivity in the East Sea (Onitsuka et al. 2007; Kim et al. 2013). Direct estimates of material transports through the straits are sparse due to the lack of concentration and transport data. Repeated observations in the eastern channel showed high nutrient transports in summer and autumn (Morimoto et al. 2009) and large interannual variability (Morimoto et al. 2012). For a complete understanding of material transports in the Korea Strait, it is necessary to conduct hydrographic observations simultaneously in both the western and eastern channels. Observations at the western channel are particularly important as the current in the western channel is stronger than that in the eastern channel (Fig. 2.8) and water masses together with materials originating from the Yellow Sea and the East China Sea mainly pass through the western channel (Chung et al. 2000; Teague et al. 2002; Takikawa et al. 2005).

There is a water mass not delivered by the TWC: Korea Strait Bottom Cold Water (KSBCW), a cold ($<10^\circ \text{C}$) water mass found mainly in the bottom layer of the western channel originating in the northern region of the East Sea (see also Sect. 3.3.2). It is observed within 70 km of the Korean coast almost throughout the year (Johnson and Teague 2002; Kim et al. 2006). Using simultaneous temperature and current data, Kim et al. (2006) showed that the bottom temperature of KSBCW decreased when the southwestward bottom current strengthened (maximum 15 cm s^{-1} of subtidal velocity). The KSBCW also exhibits interannual variations (Min et al. 2006; Na et al. 2010) associated with changes of upper water temperature, particularly in the southwestern region of the East Sea (Yun et al. 2004; Na et al. 2010).

2.4.2 Tsugaru Strait and Soya Strait

The Tsugaru Strait is about 30 km wide and 110 km long (narrower and shorter than the Korea Strait) with a sill depth of 130 m (Fig. 2.7). The eastward outflow to the Northwestern Pacific through the Tsugaru Strait is a part of the TWC system in the East Sea and is called the Tsugaru Warm Current. Continuous observation of currents across the strait using a vessel-mounted Acoustic Doppler Current Profiler

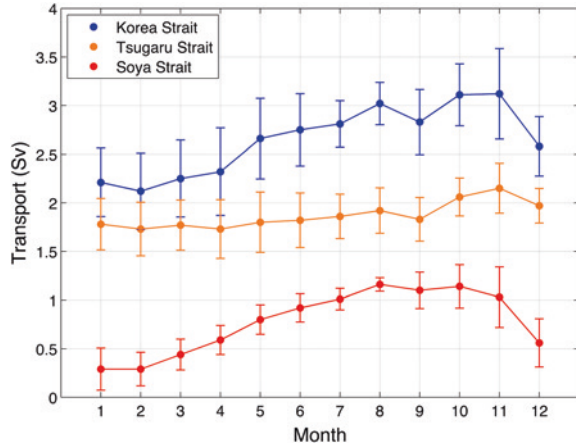
(ADCP) (Table 2.2) has improved our understanding of the mean and temporal variations of the Tsugaru Strait throughflow. Tidal currents are well known to be strong with maximum speeds exceeding 100 cm s^{-1} (Onishi et al. 2004), comparable to or greater than those in the Korea Strait. Luu et al. (2011) pointed out that the tidal residual current is not negligible (up to about 30 cm s^{-1}). Maximum subtidal current is about 130 cm s^{-1} near the middle of the strait where bottom depth is deeper than 200 m (Ito et al. 2003). Mean volume transport is estimated to be about 1.5 Sv (Toba et al. 1982; Onishi and Ohtani 1997; Ito et al. 2003; Nishida et al. 2003).

The Soya Strait is about 40 km wide and less than 20 km long with a sill depth of 55 m (narrowest, shortest, and shallowest among the three major straits). The southeastward (along the coast of Hokkaido, Fig. 2.7) outflow to the Okhotsk Sea through the Soya Strait is a part of the TWC system and is called the Soya Warm Current. Tidal currents are not strong compared to those in the Korea and Tsugaru Straits, and diurnal tidal constituents are dominant (Aota and Matsuyama 1987). Maximum subtidal currents are comparable to those in the Korea and Tsugaru Straits, being about $100\text{--}120 \text{ cm s}^{-1}$ in summer and autumn (Matsuyama et al. 2006; Ebuchi et al. 2006, 2009; Fukamachi et al. 2008, 2010). Mean transport is estimated to be about 1 Sv (Fukamachi et al. 2008) with large interannual variability (Onishi and Ohtani 1997; Fukamachi et al. 2010).

In terms of mean volume transports, outflows through the Tsugaru and Soya Straits are balanced by the inflow through the Korea Strait, thus about 60–70 % of the inflow volume flows out through the Tsugaru Strait and the rest flows out through the Soya Strait (Na et al. 2009 and references therein). However, the annual range of the transport through the Tsugaru Strait (about 0.4 Sv; Nishida et al. 2003) appears to be about half of that through the Soya Strait (about 1 Sv; Fukamachi et al. 2008). Cho et al. (2009) conducted high-resolution numerical modeling in the Northwestern Pacific region and showed that near-steady seasonal transport through the Tsugaru Strait contributes to a seasonally-varying ratio of Tsugaru Strait outflow transport to that of the Soya Strait that is high in winter and low in summer (Fig. 2.9). Seung et al. (2012) applied Godfrey's island rule (Godfrey 1989) with bottom friction and explained that the relatively small seasonal variability of Tsugaru Strait transport is because the latitude of zero-wind-stress curl over the North Pacific is located east of Hokkaido (between the Tsugaru and Soya Straits, see also Sect. 4.5).

The Tatarsky Strait is another strait, located in the northernmost region of the East Sea. Volume transport through this narrow (about 10 km) and shallow (about 10 m) strait is known to be negligible because of the cyclonic recirculation (about 2 Sv) associated with the Liman Current (Riser et al. 1999). The circulation near the Tatarsky Strait, however, could play a significant role in the freshwater budget in the East Sea, due to discharge from the Amur River (Yanagi 2002; Yoon and Kim 2009). Thus, a better knowledge of the circulation in the Tatarsky Strait may contribute to complete understanding of freshwater and salt budgets in the East Sea. Moreover, it could indirectly affect the inflow and outflow of the East Sea by altering surface circulation in the northern region (Park et al. 2006b; Yoon and Kim 2009).

Fig. 2.9 Monthly mean transports and standard deviations in the Korea, Tsugaru, and Soya straits from 1994 to 2003 derived by a primitive-equation ocean circulation model simulated for 10 years (Redrawn from Cho et al. 2009). The *vertical lines* represent standard deviations in each month



2.4.3 Long-Term Variability

Interannual to decadal variability of the boundary transports appears to be as large as seasonal variability (about 1 Sv of volume transport; Kim et al. 2004; Lyu and Kim 2005; Morimoto et al. 2012), but, compared to seasonal variability, it is not well understood. Sea level differences (SLD) from tide gauge data (Fig. 2.7) could provide multi-decadal proxies for volume transport variations and allow simultaneous comparison of the transports at different straits. SLD across the Korea Strait showed a good linear relationship with the Korea Strait volume transport (Lyu and Kim 2003; Takikawa and Yoon 2005). In the case of the Tsugaru Strait, both SLD across the Tsugaru Strait (Nishida et al. 2003) and SLD between inside and outside the East Sea (Ito et al. 2003) agreed with the Tsugaru Strait transport variations. Along-strait SLD could also be used to estimate transport variations in the case of the Soya Strait (Fukamachi et al. 2008, 2010).

Long-term time series estimates can also be used to examine relationships between East Sea variability and larger-scale variability in the Northwestern Pacific (see also Sect. 3.4). The TWC may contribute as a link between upper-ocean heat content variability in the East Sea and that in the Northwestern Pacific on a decadal time scale (Na et al. 2012). A physical-biogeochemical modeling study (Liu and Chai 2009) indicated that nutrient transport in the East Sea is connected to large-scale changes in the Pacific Decadal Oscillation (PDO), which is thought to be related to TWC variability (Gordon and Giulivi 2004), and hence to Kuroshio variability in the East China Sea (Andres et al. 2009). During positive phases of the PDO, Kuroshio transport in the East China Sea tends to decrease and TWC transport to increase, which in turn delivers more buoyant subtropical water to the East Sea. The observed long-term increasing trend of inorganic nitrogen in the East Sea is also considered to have been mainly influenced by influx through the Korea Strait (Kim et al. 2013) rather than local nitrogen flux from atmosphere (Kim et al. 2011).

2.5 Summary and Discussion

We have given an overview of current knowledge of East Sea forcings such as wind field, surface heat flux, and boundary flux through the three straits connecting to the open ocean. One of the dominant features of wind speeds in the East Sea is occasional outbreaks of very cold Siberian air. Such cold-air outbreaks through the orographic gap near Vladivostok have been studied intensively to investigate their impacts on the circulation in the basin. They play an important role in generating cold bottom water formation south of the Peter the Great Bay (see Fig. 1.1) through brine rejection during sea ice formation (Talley et al. 2003). In addition, they have a significant effect on the circulation of the cyclonic gyre in the Japan Basin. Wind stress curl and divergence fields in the path of cold continental air outbreaks are modified by wind-sea surface temperature coupling across the sub-polar front due to changes in MABL stability.

In contrast with the cold-air outbreak through Vladivostok, the role of strong winds over East Korea Bay during the outbreak period has not been thoroughly studied. The winds are expected to control relatively small-scale cyclonic and anti-cyclonic circulation and mesoscale eddies in the local region. In addition, the relationship between wind forcings and subpolar frontal dynamics should be further investigated (Yoshikawa et al. 2012). SST-wind coupling and its feedback mechanisms near the frontal region have not been vigorously studied and need further studies. Year-to-year variation and long-term variability of wind forcing and its relation to climate change should be studied continuously. Issues related to climate change and local changes in wind forcings should be also considered further in the future.

The East Sea gains heat from April to August and loses heat in the other months. The annual mean net heat flux is negative with a large range of $25\text{--}108\text{ W m}^{-2}$ according to previous estimates. The East Sea's inflow–outflow system compensates for the net heat loss. The winter (December–February) net heat losses, which are important in deep water formation in the northern East Sea and frontal subduction along the subpolar front, range from $250\text{ to }330\text{ W m}^{-2}$. Latent and sensible heat fluxes are mainly responsible for net heat losses in winter due to the winter monsoon with intermittent strong cold-air outbreaks. The net loss becomes enhanced when cold and dry air sweeps over the warm sea surface south of the subpolar front; this results in spatial differences in net and latent heat fluxes in winter. In summer, the net heat flux is mainly determined by radiation components, with heat loss components, including long wave cooling, showing their annual minima. The summertime (June–August) net heat flux ranges from $90\text{ to }155\text{ W m}^{-2}$.

Heat flux estimates presented here share some common features, such as their seasonal variations, but there are also considerable quantitative differences in all heat flux components. Interannual variation and long-term trends of surface heat fluxes are poorly known in the East Sea, although many studies have documented long-term changes and variability of deep water masses that are mainly formed

in the northern East Sea during winter. It needs to be determined whether or not long-term variabilities of water properties and deep circulation are associated with varying surface air-sea fluxes. Atmospheric reanalysis products have been widely used to understand spatiotemporal variation of air-sea fluxes; they will also be very useful in the East Sea, but must be used with caution. Intercomparison of different products, and quantitative evaluation of the products based on in situ measurements, are prerequisites in the use of any specific product.

There has been significant progress in understanding boundary flux in the East Sea since continuous monitoring started in the late 1990s or early 2000s, along with extensive studies of currents and circulation in the straits. Outflows through the Tsugaru and Soya Straits are closely linked with inflow through the Korea Strait (2.6 Sv) because of the semi-enclosed nature of the East Sea and negligible flow through the Tatarsky Strait. Seasonally, the inflow and outflows are generally large in summer to autumn and small in winter to spring with the range of about 1 Sv. Seasonal variability in the Korea Strait tends to be reflected more in the Soya Strait rather than in the Tsugaru Strait, although mean outflow through the Tsugaru Strait is larger than that through the Soya Strait (Fig. 2.9). The TWC system in the East Sea is controlled by large-scale and local wind forcing on time scales longer than a month. Interannual variability (comparable to seasonal variability) and decadal variability of the TWC system needs further study along with its relationship to Northwestern Pacific variability.

Material transports in the East Sea have been less studied than volume transports, because of limited observations. Although strongly related to volume transport through the straits, other factors, such as intrusion of different water masses, alter material transport significantly. Moreover, comparison of material transports at different straits has been very limited. Thus, simultaneous observations at the straits including hydrographic and biogeochemical sampling is most needed for future progress in understanding boundary transports in the East Sea.

Acknowledgments Authors would like to thank Eun-Young Lee (Seoul National University) for her editorial work. This study was supported partly by EAST-I project of the Ministry of Oceans and Fisheries of Korea.

References

- Ahn JB, Ryu JH, Yoon YH (1997) Comparative analysis and estimates of heat fluxes over the ocean around Korean Peninsula. *J Korean Meteorol Soc* 33:725–736 (in Korean)
- Andres M, Wimbush M, Park JH et al (2008) Observations of Kuroshio flow variations in the East China Sea. *J Geophys Res* 113:C05013. doi:[10.1029/2007JC004200](https://doi.org/10.1029/2007JC004200)
- Andres M, Park JH, Wimbush M et al (2009) Manifestation of the Pacific decadal oscillation in the Kuroshio. *Geophys Res Lett* 36:116602. doi:[10.1029/2009GL039216](https://doi.org/10.1029/2009GL039216)
- Aota M, Matsuyama M (1987) Tidal current fluctuations in the Soya Current. *J Oceanogr Soc Jpn* 43:276–282
- Beardsley RC, Limeburner R, Yu H et al (1985) Discharge of the Changjiang (Yangtze River) into the East China Sea. *Cont Shelf Res* 4:57–76

- Berry DI, Kent EC (2009) A new air-sea interaction gridded dataset from ICOADS with uncertainty estimates. *Bull Am Meteorol Soc* 90:645–656
- Cardone VJ (1969) Specification of the wind field distribution in the marine boundary layer for wave forecasting. New York University, New York
- Chang KI, Teague WJ, Lyu SJ et al (2004) Circulation and currents in the southwestern East/Japan Sea: overview and review. *Prog Oceanogr* 61:105–156
- Chelton DB, Schlax MG, Freilich MH et al (2004) Satellite measurements reveal persistent small-scale features in ocean winds. *Science* 303:978–983
- Chen C, Beardsley RC, Limeburner R et al (1994) Comparison of winter and summer hydrographic observations in the yellow and East China Sea and adjacent Kuroshio during 1986. *Cont Shelf Res* 14:909–929
- Chen SS, Zhao W, Tenerelli JE et al (2001) Impact of the AVHRR sea surface temperature on atmospheric forcing in the Japan/East Sea. *Geophys Res Lett* 28:4539–4542
- Cho YK, Seo GH, Choi BJ et al (2009) Connectivity among straits of the northwest Pacific marginal seas. *J Geophys Res* 114:C06018. doi:[10.1029/2008JC005218](https://doi.org/10.1029/2008JC005218)
- Cho YK, Seo GH, Kim CS et al (2013) Role of wind stress in causing maximum transport through the Korea Strait in autumn. *J Mar Syst* 115–116:33–39
- Chu PC, Lan J, Fan C (2001) Japan Sea thermohaline structure and circulation part I: climatology. *J Phys Oceanogr* 31:244–271
- Chung CS, Hong GH, Kim SH et al (2000) Biogeochemical fluxes through the Cheju Strait. *J Korean Soc Oceanogr* 5:208–215
- Dorman CE, Beardsley RC, Dashko NA et al (2004) Winter marine atmospheric conditions over the Japan Sea. *J Geophys Res* 109:C12011. doi:[10.1029/2001JC001197](https://doi.org/10.1029/2001JC001197)
- Dorman CE, Beardsley RC, Limeburner R et al (2005) Summer atmospheric conditions over the Japan/East Sea. *Deep-Sea Res Part II* 52:1393–1420
- Ebuchi N (1997) Statistical distribution of wind speeds and directions contained in the preliminary NSCAT science data products. *J Adv Mar Sci Tech Soc* 3(2):141–156
- Ebuchi N, Fukamachi Y, Ohshima KI et al (2006) Observation of the Soya warm current using HF ocean radar. *J Oceanogr* 62:47–61
- Ebuchi N, Fukamachi Y, Ohshima KI et al (2009) Subinertial and seasonal variations in the Soya Warm Current revealed by HF ocean radars, coastal tide gauges, and bottom-mounted ADCP. *J Oceanogr* 65:31–43
- Fang G, Zhao B, Zhu Y (1991) Water volume transport through the Taiwan Strait and the continental shelf of the East China Sea measured with current meters. In: Takano K (ed) *Oceanography: Asian marginal seas*. Elsevier, New York, pp 345–358
- Freilich MH (1997) Validation of vector magnitude datasets: effects of random component errors. *J Atmos Ocean Technol* 14:695–703
- Fukamachi Y, Tanaka I, Ohshima KI et al (2008) Volume transport of the Soya Warm Current revealed by bottom-mounted ADCP and ocean-radar measurement. *J Oceanogr* 64:385–392
- Fukamachi Y, Ohshima KI, Ebuchi N et al (2010) Volume transport in the Soya Strait during 2006–2008. *J Oceanogr* 66:685–696
- Godfrey JS (1989) A Sverdrup model of the depth-integrated flow from the world ocean allowing for island circulations. *Geophys Astrophys Fluid Dyn* 45:89–112
- Gordon AL, Giulivi CF (2004) Pacific decadal oscillation and sea level in the Japan/East Sea. *Deep-Sea Res Part I* 51:653–663
- Han IS, Kang YQ (2003) Supply of heat by Tsushima Warm Current in the East Sea (Japan Sea). *J Oceanogr* 59:317–323
- Hirose N, Kim CH, Yoon JH (1996) Heat budget in the Japan Sea. *J Oceanogr* 52:553–574
- Hogan PJ, Hulbert HE (2000) Impact of upper ocean-topographical coupling and isopycnal outcropping in Japan/East Sea models with 1/8° to 1/64° resolution. *J Phys Oceanogr* 30:2535–2561
- Hong GM, Kwon BH, Kim YS (2005) Heat fluxes in the marine atmospheric surface layer around the Korean Peninsula based on satellite data. *J Fish Mar Sci Educ* 29:210–217 (in Korean)

- Isobe A (2008) Recent advances in ocean-circulation research on the Yellow Sea and East China Sea shelves. *J Oceanogr* 64:569–584
- Isobe A, Tawara S, Kaneko A et al (1994) Seasonal variability in the Tsushima Warm Current, Tsushima-Korea Strait. *Cont Shelf Res* 14:23–35
- Isobe A, Ando M, Watanabe T et al (2002) Freshwater and temperature transports through the Tsushima-Korea Straits. *J Geophys Res* 107:C73065. doi:[10.1029/2000JC000702](https://doi.org/10.1029/2000JC000702)
- Isoda Y (1999) Cooling-induced current in the upper ocean of the Japan Sea. *J Oceanogr* 55:585–596
- Isoguchi O, Kawamura H (2007) Coastal wind jets flowing into the Tsushima Strait and their effect on wind-wave development. *J Atmos Sci* 64:564–578
- Ito T, Togawa O, Ohnishi M et al (2003) Variation of velocity and volume transport of the Tsugaru Warm Current in the winter of 1999–2000. *Geophys Res Lett* 30(13):1678. doi:[10.1029/2003GL017522](https://doi.org/10.1029/2003GL017522)
- Jet Propulsion Laboratory (1998) Science data product (NSCAT-2) user's manual ver 1.2. In: Overview and geophysical data products. Jet Propulsion Laboratory, Pasadena
- Johnson DR, Teague WJ (2002) Observations of the Korea Strait bottom cold water. *Cont Shelf Res* 22:821–831
- Kato K, Asai T (1983) Seasonal variations of heat budgets in both the atmosphere and the sea in the Japan Sea area. *J Meteorol Soc Japan* 61:222–237
- Kawamura H, Wu P (1998) Formation mechanism of Japan Sea proper water in the flux center off Vladivostok. *J Geophys Res* 103(C10):21611–21622
- Kim SB, Fukumori I (2008) A near uniform basin-wide sea level fluctuation over the Japan/East Sea: a semienclosed sea with multiple Straits. *J Geophys Res* 113:C06031. doi:[10.1029/2007JC004409](https://doi.org/10.1029/2007JC004409)
- Kim DJ, Moon WM (2002) Estimation of sea surface wind vector using RADARSAT data. *Remote Sens Environ* 80(1):55–64
- Kim TS, Park KA (2011) Estimation of polarization ratio for sea surface wind retrieval from SIR-C SAR data. *Korean J Remote Sens* 27(6):729–741
- Kim CH, Yoon JH (1996) Modeling of the wind-driven circulation in the Japan Sea using a reduced gravity model. *J Oceanogr* 52(3):359–373
- Kim KR, Kim G, Kim K et al (2002) A sudden bottom water formation during the severe winter 2000–2001: the case of the East/Japan Sea. *Geophys Res Lett* 29(8):1234. doi:[10.1029/2001GL014498](https://doi.org/10.1029/2001GL014498)
- Kim K, Lyu SJ, Kim YG et al (2004) Monitoring volume transport through measurement of cable voltage across the Korea Strait. *J Atmos Ocean Technol* 21:671–682
- Kim K, Kim YB, Park JJ et al (2005) Long-term and real-time monitoring system of the East/Japan Sea. *Ocean Sci J* 40(1):25–44
- Kim YH, Kim YB, Kim K et al (2006) Seasonal variation of the Korea Strait bottom cold water and its relation to the bottom current. *Geophys Res Lett* 33:L24604. doi:[10.1029/2006GL027625](https://doi.org/10.1029/2006GL027625)
- Kim TS, Park KA, Moon WI (2010) Wind vector retrieval from SIR-C SAR data off the east coast of Korea. *J Korean Earth Sci Soc* 31(5):475–487
- Kim TW, Lee K, Najjar RG et al (2011) Increasing N abundance in the Northwestern Pacific Ocean due to atmospheric nitrogen deposition. *Science* 334:504–509
- Kim TS, Park KA, Choi WM et al (2012) L-band SAR-derived sea surface wind retrieval off the east coast of Korea and error characteristics. *Korean J Remote Sens* 28(5):477–487
- Kim SK, Chang KI, Kim B et al (2013) Contribution of ocean current to the increase in N abundance in the northwestern Pacific marginal seas. *Geophys Res Lett* 40:143–148. doi:[10.1029/2012GL054545](https://doi.org/10.1029/2012GL054545)
- Kondo T, Ostrovskii A, Umatani S (1994) Climatologies of the heat fluxes over the Japan Sea. In: Proceedings of CREAMS'94 international symposium
- Kuroda H, Isoda Y, Ohnishi M et al (2004) Examination of harmonic analysis methods using semi-regular sampling data from an ADCP installed on a regular ferry: evaluation of tidal and residual currents in the eastern mouth of the Tsugaru Strait. *Umi no Kenkyu* 13:553–564 (in Japanese)

- Lee DK (1998) Ocean surface winds over the seas around Korea measured by the NSCAT (NASA Scatterometer). *J Korean Soc Remote Sens* 14(1):37–52 (in Korean)
- Li G, Ren B, Zheng J et al (2011) Net air-sea surface heat flux during 1984–2004 over the North Pacific and North Atlantic oceans (10°N–50°N): annual mean climatology and trend. *Theor Appl Climatol* 104:387–401
- Lie HJ, Cho CH, Lee JH et al (1998) Separation of the Kuroshio water and its penetration onto the continental shelf west of Kyushu. *J Geophys Res* 103:2963–2976
- Liu G, Chai F (2009) Seasonal and interannual variation of physical and biological processes during 1994–2001 in the Sea of Japan/East Sea: a three-dimensional physical-biogeochemical modeling study. *J Mar Syst* 78:265–277
- Liu WT, Xie X (2006) Measuring ocean surface wind from space. In: Gower J (ed) *Remote sensing of the marine environment, manual of remote sensing*, vol 6, 3rd edn., American Society for photogrammetry and remote sensing Bethesda, USA, pp 149–178
- Liu N, Eden C, Dietze H et al (2010) Model-based estimate of the heat budget in the East China Sea. *J Geophys Res* 115:C08026. doi:[10.1029/2009JC005869](https://doi.org/10.1029/2009JC005869)
- Luu QH, Ito K, Ishikawa Y et al (2011) Tidal transport through the Tsugaru Strait—part 1: characteristics of the major tidal flow and its residual current. *Ocean Sci J* 46:273–288
- Lyu SJ, Kim K (2003) Absolute transport from sea level difference across the Korea Strait. *Geophys Res Lett* 30(6):1285. doi:[10.1029/2002GL016233](https://doi.org/10.1029/2002GL016233)
- Lyu SJ, Kim K (2005) Subinertial to interannual transport variations in the Korea Strait and their possible mechanisms. *J Geophys Res* 110:C12016. doi:[10.1029/2004JC002651](https://doi.org/10.1029/2004JC002651)
- Lyu SJ, Kim K, Perkins HT (2002) Atmospheric pressure-forced subinertial variations in the transport through the Korea Strait. *Geophys Res Lett* 29(9):1294. doi:[10.1029/2001GL014366](https://doi.org/10.1029/2001GL014366)
- Ma C, Wu D, Lin X et al (2012) On the mechanism of seasonal variation of the Tsushima Warm Current. *Cont Shelf Res* 48:1–7
- Matsuyama M, Wadaka M, Abe T et al (2006) Current structure and volume transport of the Soya Warm Current in summer. *J Oceanogr* 62:197–205
- Min HS, Kim YH et al (2006) Year-to-year variation of cold waters around the Korea Strait. *Ocean Sci J* 41:227–234
- Moon JH, Hirose N, Yoon J-H et al (2009) Effect of the along-strait wind on the volume transport through the Tsushima/Korea Strait in September. *J Oceanogr* 65:17–29
- Morimoto A, Takikawa T, Onitsuka G et al (2009) Seasonal variation of horizontal material transport through the eastern channel of the Tsushima Straits. *J Oceanogr* 65:61–71
- Morimoto A, Watanabe A, Onitsuka G et al (2012) Interannual variations in material transport through the eastern channel of the Tsushima/Korea Straits. *Prog Oceanogr* 105:38–46
- Na JY, Han SK, Seo JW et al (1997) Empirical orthogonal function analysis of surface pressure, sea surface temperature and winds over the East Sea of Korea (Japan Sea). *J Korean Fish Soc* 30:188–202 (in Korean)
- Na J, Seo J, Lie HJ (1999) Annual and seasonal variations of the sea surface heat fluxes in the East Asian marginal seas. *J Oceanogr* 55:257–270
- Na H, Isoda Y, Kim K et al (2009) Recent observations in the straits of the East/Japan Sea: a review of hydrography, currents and volume transports. *J Mar Syst* 78(2):200–205
- Na H, Kim KY, Chang KI et al (2010) Interannual variability of the Korea Strait bottom cold water and its relationship with the upper water temperatures and atmospheric forcing in the Sea of Japan (East Sea). *J Geophys Res* 115:C09031. doi:[10.1029/2010JC006347](https://doi.org/10.1029/2010JC006347)
- Na H, Kim KY, Chang KI et al (2012) Decadal variability of the upper-ocean heat content in the East/Japan Sea and its relationship to Northwestern Pacific variability. *J Geophys Res* 117:C02017. doi:[10.1029/2011JC007369](https://doi.org/10.1029/2011JC007369)
- Nam SH, Lyu SJ, Kim YH et al (2004) Correction on TOPEX/POSEIDON altimeter data for nonisostatic sea level response to atmospheric pressure in the Japan/East Sea. *Geophys Res Lett* 31:L02304. doi:[10.1029/2003GL018487](https://doi.org/10.1029/2003GL018487)
- Nam SH, Kim YH, Park KA et al (2005) Spatio-temporal variability in sea surface wind stress near and off the east coast of Korea. *Acta Oceanol Sin* 24(1):107–114

- Nishida Y, Kanomata I, Tanaka I et al (2003) Seasonal and interannual variations of the volume transport through the Tsugaru Strait. *Umi no Kenkyu* 12:487–499 (in Japanese)
- Nitani H (1972) Beginning of the Kuroshio. In: Yoshida K (ed) *Stommel H. Its physical aspects*. University of Tokyo press, Kuroshio, pp 129–163
- Onishi M, Ohtani K (1997) Volume transport of the Tsushima Warm Current, west of Tsugaru Strait bifurcation area. *J Oceanogr* 53:27–34
- Onishi M, Isoda Y, Kuroda H et al (2004) Winter transport and tidal current in the Tsugaru Strait. *Bull Fish Sci Hokkaido Univ* 55:105–119
- Onitsuka G, Yanagi T, Yoon JH (2007) A numerical study on nutrient sources in the surface layer of the Japan Sea using a coupled physical-ecosystem model. *J Geophys Res* 112:C05042. doi:[10.1029/2006JC003981](https://doi.org/10.1029/2006JC003981)
- Park KA, Cornillon PC (2002) Stability-induced modification of sea surface wind over Gulf Stream rings. *Geophys Res Lett* 29(24):2211. doi:[10.1029/2001GL014236](https://doi.org/10.1029/2001GL014236)
- Park JH, Watts DR (2005) Response of the southwestern Japan/East Sea to atmospheric pressure. *Deep-Sea Res Part II* 52:1671–1683
- Park W, Oh IS, Shim T (1995) Temporal and spatial distributions of heat fluxes in the East Sea (Sea of Japan). *J Korean Soc Oceanogr* 30:91–115 (in Korean)
- Park KA, Kim KR, Chung JY et al (2003) Comparison of the wind speed from an atmospheric pressure map (Na wind) and satellite scatterometer-observed wind speed (NSCAT) over the East (Japan) Sea. *J Korean Soc Oceanogr* 38(4):173–184
- Park KA, Cornillon PC, Codiga DL (2006a) Modification of surface winds near ocean fronts: effects of Gulf Stream rings on scatterometer (QuikSCAT, NSCAT) wind observations. *J Geophys Res* 111:C03021. doi:[10.1029/2005JC003016](https://doi.org/10.1029/2005JC003016)
- Park KA, Kim K, Cornillon PC et al (2006b) Relationship between satellite-observed cold water along the Primorye coast and sea ice in the East Sea (the Sea of Japan). *Geophys Res Lett* 33:L10602. doi:[10.1029/2005GL025611](https://doi.org/10.1029/2005GL025611)
- Park YG, Yeh SW, Hwang JH et al (2013) Origin of the Tsushima Warm Current in a high resolution ocean circulation model. *J Coast Res* 65:2041–2046
- Riser SC, Warner MJ, Yurasov GI (1999) Circulation and mixing of water masses of Tatar Strait and the northwestern boundary region of the Japan Sea. *J Oceanogr* 55:133–156
- Senjyu T, Enomoto H, Matsuno T et al (2006) Interannual salinity variations in the Tsushima Strait and its relation to the Changjiang discharge. *J Oceanogr* 62:681–692
- Senjyu T, Han IS, Matsui S (2009) Connectivity between the interannual salinity variation in the western channel of the Tsushima Strait and hydrographic conditions in the Cheju Strait. *J Oceanogr* 65:511–524
- Seung YH, Han SY, Lim EP (2012) Seasonal variation of volume transport through the straits of the East/Japan Sea viewed from the Island rule. *Ocean Polar Res* 34:403–411
- Shimada T, Kawamura H (2006) Satellite observations of sea surface temperature and sea surface wind coupling in the Japan Sea. *J Geophys Res* 111:C08010. doi:[10.1029/2005JC003345](https://doi.org/10.1029/2005JC003345)
- Takikawa T, Yoon JH (2005) Volume transport through the Tsushima Straits estimated from sea level difference. *J Oceanogr* 61:699–708
- Takikawa T, Yoon JH, Cho KD (2003) Tidal currents in the Tsushima Straits estimated from ADCP data by ferryboat. *J Oceanogr* 59:37–47
- Takikawa T, Yoon JH, Cho KD (2005) The Tsushima Warm Current through Tsushima Straits estimated from ferryboat ADCP data. *J Phys Oceanogr* 35:1154–1168
- Talley LD, Lobanov V, Ponomarev V et al (2003) Deep convection and brine rejection in the Japan Sea. *Geophys Res Lett* 30(4):1159. doi:[10.1029/2002GL016451](https://doi.org/10.1029/2002GL016451)
- Teague WJ, Jacobs GA, Perkins HT et al (2002) Low frequency current observations in the Korea/Tsushima Strait. *J Phys Oceanogr* 32:1621–1641
- Teague WJ, Hwang PA, Jacobs GA et al (2005) Transport variability across the Korea/Tsushima Strait and the Tsushima Island wake. *Deep-Sea Res Part II* 52:1784–1801
- Teague WJ, Ko DS, Jacobs JA et al (2006) Currents through the Korea/Tsushima Strait: a review of LINKS observations. *Oceanography* 19:50–63

- Toba Y, Tomizawa K, Kurasawa Y et al (1982) Seasonal and year-to-year variability of the Tsushima-Tsugaru Warm Current System with its possible cause. *La Mer* 20:41–51
- Trusenkova O, Nikitin A, Lobanov V (2009) Circulation features in the Japan/East Sea related to statistically obtained wind patterns. *J Mar Syst* 78:214–225
- Tsujino H, Nakano H, Motoi T (2008) Mechanism of currents through the straits of the Japan Sea: mean state and seasonal variation. *J Oceanogr* 64:141–161
- Yanagi T (2002) Water, salt, phosphorus and nitrogen budgets of the Japan Sea. *J Oceanogr* 58:797–804
- Yoon JH, Kim YJ (2009) Review on the seasonal variation of the surface circulation in the Japan/East Sea. *J Mar Syst* 78:226–236
- Yoon JH, Abe K, Ogata T et al (2005) The effects of wind-stress curl on the Japan/East Sea circulation. *Deep-Sea Res Pt II* 52:1827–1844
- Yoshikawa Y, Masuda A, Marubayashi K et al (2006) On the accuracy of HF radar measurement in the Tsushima Strait. *J Geophys Res* 111:C04009. doi:[10.1029/2005JC003232](https://doi.org/10.1029/2005JC003232)
- Yoshikawa Y, Masuda A, Marubayashi K et al (2010) Seasonal variations of the surface currents in the Tsushima Strait. *J Oceanogr* 66:223–232
- Yoshikawa Y, Lee CM, Thomas LN (2012) The subpolar front of the Japan/East Sea part III: competing roles of frontal dynamics and atmospheric forcing in driving ageostrophic vertical circulation and subduction. *J Phys Oceanogr* 42:991–1011
- Yu L, Weller RA (2007) Objectively analyzed air-sea fluxes for the global ice-free oceans (1981–2005). *Bull Am Meteorol Soc* 88:527–539
- Yun JY, Magaard L, Kim K et al (2004) Spatial and temporal variability of the North Korean cold water leading to the near-bottom cold water intrusion in Korea Strait. *Prog Oceanogr* 60:99–131
- Zhang Q, Hou Y, Yan T (2012) Inter-annual and inter-decadal variability of Kuroshio heat transport in the East China Sea. *Int J Climatol* 32:481–488

Oceanography of the East Sea (Japan Sea)

Chang, K.-I.; Zhang, C.-I.; Park, C.; Kang, D.-J.; Ju, S.-J.;

Lee, S.-H.; Wimbush, M. (Eds.)

2016, XVI, 460 p., Hardcover

ISBN: 978-3-319-22719-1